Dimension Reduction and Tabulation of Combustion Chemistry using ICE-PIC and ISAT

Zhuyin Ren*, Varun Hiremath†, Stephen B. Pope†
*ANSYS, Inc., 10 Cavendish Court, Lebanon, NH 03766, USA
†Cornell University, Mechanical & Aerospace Engineering, Ithaca, NY 14853, USA

***Abstract*— Progress is reported in the integration of two methodologies to enable the efficient application of realistic combustion chemistry in computational fluid dynamics. These methodologies are ICE-PIC (invariant constrained-equilibrium edge manifold using the pre-image curve method) for dimension reduction, and ISAT (*in situ* adaptive tabulation) for tabulation of the reduced system. New results are reported on the tangent vectors of the constrained-equilibrium and ICE manifolds, which are important quantities in ICE-PIC/ISAT. The test case of a partially-stirred reactor with methane combustion is used to demonstrate the accuracy and efficiency of the combined approach.**

I. Introduction

Dimension reduction is essential to the use of detailed chemical kinetics in computations of combustion and many other reactive flows. Modern chemical mechanisms for hydrocarbon fuel may contain of order 1,000 species [1], and it is clearly impracticable to use this detailed information directly in multi-dimensional computational fluid dynamics (CFD) calculations. A combination of three approaches that enables the use of detailed chemical information consists of: (1) reduction to a skeletal mechanism [2], [3], [4] involving of order 100 species; (2) dimension reduction (DR) to reduce the number of degrees of freedom to of order ten; and (3) tabulation to significantly reduce the cost of expensive evaluations, e.g., the integration of ordinary differential equations (ODEs).

In this work we develop a general, combined dimension reduction/tabulation methodology by considering the integration of two successful techniques, namely, the invariant constrained-equilibrium edge pre-image curve (ICE-PIC) method for dimension reduction [5], [6], [7], and *in situ* adaptive tabulation (ISAT) [8], [9]. An example of the application of this type of methodology is as follows. A detailed mechanism with n_s species is provided. In the reduced description given by ICE-PIC/ISAT, the reactive flow calculation is performed in terms of a small number of n_r reduced variables, and chemical reaction is separated from other processes into a reaction fractional step, by using a splitting scheme. Given the reduced variables at time t, the task in this reaction fractional step is to determine the corresponding reduced variables after (adiabatic, isobaric) reaction has occurred for the time-step interval. The ISAT algorithm, a storage/retrieval technique, tabulates the reduced variable information before and after reaction, so that, given the reduced variables before the reaction substep, the corresponding values after reaction can be retrieved from the table. Only when needed, ISAT adds new entries to the table by invoking the ICE-PIC dimension reduction procedure together with the detailed mechanisms. In other words, the reduction/tabulation methodology determines and tabulates (*in situ*) the necessary information about the n_r-dimensional reduced system based on the n_s-species detailed mechanism.

In the next section we briefly review the ICE-PIC method as implemented in conjunction with ISAT. Then we derive expressions for the tangent vectors of the constrained-equilibrium manifold (CEM) and the ICE manifold, which are needed by ISAT. Finally, results are given for the test case of a partially-stirred reactor with methane combustion, showing the accuracy of the dimension reduction and the efficiency gains achieved by ISAT.

II. The ICE-PIC Method

The ICE-PIC dimension reduction method is based on constrained equilibrium theory [10], [11], [12], trajectory-generated manifolds [13] and the pre-image curve method [14]. We give here a succinct overview of the ICE-PIC method, as it is implemented in conjunction with ISAT. More details can be found in [5], [6], [7].

We consider a gas-phase mixture of n_s chemical species composed of n_e elements. The thermochemical state of the mixture (at a given position and time) is completely characterized by the pressure p, the mixture enthalpy h, and the n_s-vector $\mathbf{z}$ of the specific moles of the species. To simplify the exposition, we take p and h to be given constants, and so the state is given by $\mathbf{z}$.

Due to chemical reactions, the composition evolves by

$$\frac{d\mathbf{z}}{dt} = \mathbf{S}(\mathbf{z}), \tag{1}$$

where $\mathbf{S}$ is the n_s-vector of chemical production rates. The "reaction mapping" $\mathbf{R}(\mathbf{z}, t)$ is defined to be the solution to (1) after time t from the initial condition $\mathbf{z}$. And the mapping gradient $\mathbf{A}(\mathbf{z}, t)$ is the $n_s \times n_s$ matrix with components

$$A_{ij} = \partial R_i / \partial z_j. \tag{2}$$

In practice $\mathbf{R}$ and $\mathbf{A}$ are obtained together using the ODE solver DASAC [15].

In the ICE-PIC method, the species are decomposed as $\mathbf{z} = \{\mathbf{z}^r, \mathbf{z}^u\}$, where $\mathbf{z}^r$ is an n_{rs} vector of "represented" species, and $\mathbf{z}^u$ is an n_{us}-vector of "unrepresented"

species (with $n_{rs} + n_{us} = n_s$ and $n_{rs} < n_s - n_e$). At the present stage of development of the methodology, the represented species are specified: ultimately, the methodology should identify the optimal specification. The "reduced representation" of the species used in ICE-PIC is $\mathbf{r} \equiv \{\mathbf{z}^r, \mathbf{z}^{u,e}\}$, where $\mathbf{z}^{u,e}$, is an n_e-vector giving the specific moles of the elements in the unrepresented species. Thus $\mathbf{r}$ is a vector of length $n_r = n_{rs} + n_e$, and the dimensions of the system is reduced from n_s to $n_r < n_s$. This dimension reduction process can be written

$$\mathbf{r} = \mathbf{B}^T \mathbf{z}, \tag{3}$$

where $\mathbf{B}$ is a known constant $n_s \times n_r$ matrix.

The fundamental issue in dimension reduction of combustion chemistry is "species reconstruction" that is, given $\mathbf{r}$, define an appropriate full composition $\mathbf{z}$. We denote by $\mathbf{z}^{ICE}(\mathbf{r})$ the species reconstruction given by the ICE-PIC method. We also consider $\mathbf{z}^{CE}(\mathbf{r})$ which is the constrained-equilibrium (maximum-entropy) composition, as used in the rate-controlled constrained equilibrium method (RCCE, [10], [11], [12]). This is readily computed using the constrained-equilibrium code CEQ [16].

In the n_s-dimensional full space, the "realizable region" is the simplex defined by $z_i \geq 0$, $\mathbf{w}^T\mathbf{z} = 1$, where $\mathbf{w}$ is the n_s-vector of molecular weights. (The normalization condition $\mathbf{w}^T\mathbf{z} = 1$ is equivalent to the mass fractions summing to unity.) Thus, the realizable region for $\mathbf{z}$ is a simplex in the $(n_s - 1)$-dimensional affine space $\mathbf{w}^T\mathbf{z} = 1$, which has n_s facets (corresponding to $z_i = 0$, $i = 1, \cdots, n_s$). In the n_r-dimensional reduced space, the "realizable region" corresponds to $\mathbf{r} = \mathbf{B}^T\mathbf{z}$ for all realizable $\mathbf{z}$. This is a convex polytope within which the components of $\mathbf{r}$ are non-negative. The boundary of this reduced realizable region may have very many facets, but, in the applications described below, the facets encountered usually correspond to one component of $\mathbf{r}$ being zero. The "constrained equilibrium edge" is defined as $\mathbf{z}^{CE}(\mathbf{r})$ for all $\mathbf{r}$ on the boundary. The ICE manifold is defined as $\mathbf{R}(\mathbf{z}^{CE}(\mathbf{r}), t)$ for all $\mathbf{r}$ on the boundary and all $t \geq 0$. Thus the ICE manifold is the trajectory-generated manifold originating from all the constrained equilibrium compositions on the boundary. Some important properties of the ICE manifold are:

1) existence: for all realizable $\mathbf{r}$ there exists a manifold point $\mathbf{z}^{ICE}(\mathbf{r})$
2) invariance: the ICE manifold is invariant with respect to (1)
3) continuity: the ICE manifold is continuous
4) smoothness: the ICE manifold is piecewise smooth, and is the union of smooth manifolds generated by the facets
5) uniqueness: for a reasonable specification of the represented species, the manifold is not "folded", so that for given $\mathbf{r}$ there is a unique manifold point $\mathbf{z}^{ICE}(\mathbf{r})$.

Provided that the manifold is not folded, given a realizable value of $\mathbf{r}$, there is a unique "generating boundary point" $\mathbf{r}^g$, and time τ such that

$$\mathbf{z}^{ICE}(\mathbf{r}) = \mathbf{R}(\mathbf{z}^{CE}(\mathbf{r}^g), \tau). \tag{4}$$

The pre-image curve method [14] is used to identify $\mathbf{r}^g$ (given $\mathbf{r}$) and consequently the unique ICE manifold point $\mathbf{z}^{ICE}(\mathbf{r})$. Of course, consistency conditions are

$$\mathbf{B}^T\mathbf{z}^{ICE}(\mathbf{r}) = \mathbf{B}^T\mathbf{z}^{CE}(\mathbf{r}) = \mathbf{r}. \tag{5}$$

III. The CEM Tangent Vectors and the ICE Manifold Tangent Vectors

In the combined ICE-PIC/ISAT approach, the tabulation is performed *in situ* during the combustion calculations and is made in the n_r-dimensional reduced space. Important quantities needed in the approach are the tangent vectors of the ICE manifold. Here, we present some new theoretical results which provide quite simple means of determining the tangent vectors of the constrained-equilibrium and ICE manifolds.

A. The CEM Tangent Vectors

An important quantity in the ICE-PIC method is the $n_s \times n_r$ matrix $\mathbf{T}^{CE}$ whose columns span the tangent space of the CE manifold, and which relates infinitesimal changes in $\mathbf{z}^{CE}$ to those in $\mathbf{r}$ by

$$d\mathbf{z}^{CE} = \mathbf{T}^{CE} d\mathbf{r}. \tag{6}$$

We have obtained a new, simple expression for $\mathbf{T}^{CE}$. It is presented here for the case of fixed pressure and temperature, from which the corresponding result for fixed p and h is readily obtained.

For the case considered, the constrained equilibrium composition is given by [16]

$$\mathbf{z}^{CE} = \bar{N} \exp\left(-\tilde{\mathbf{g}} + \mathbf{B}\boldsymbol{\lambda}\right), \tag{7}$$

where $\bar{N} = \sum_{i=1}^{n_s} z_i^{CE}$ is the specific moles of all species; $\tilde{\mathbf{g}}$ are normalized Gibbs functions; and $\boldsymbol{\lambda}$ are constraint potentials (or Lagrange multipliers).

Considering infinitesimals, we obtain from (7)

$$d\mathbf{z}^{CE} = \mathbf{z}^{CE} d\,\ln(\bar{N}) + \mathbf{Z}\mathbf{B} d\boldsymbol{\lambda}, \tag{8}$$

where $\mathbf{Z}$ is the diagonal matrix formed from $\mathbf{z}^{CE}$. Summing (8) over all the species leads to the constraint

$$0 = \mathbf{z}^T\mathbf{B} d\boldsymbol{\lambda} = \mathbf{r}^T d\boldsymbol{\lambda}. \tag{9}$$

Equation (8) can be re-expressed as

$$d\mathbf{z}^{CE} = \mathbf{M} d\hat{\boldsymbol{\lambda}}, \tag{10}$$

with

$$d\hat{\boldsymbol{\lambda}} \equiv d\boldsymbol{\lambda} + \frac{\mathbf{r} d\bar{N}}{|\mathbf{r}|^2 \bar{N}}, \tag{11}$$

and

$$\mathbf{M} \equiv \mathbf{z}\mathbf{r}^T + \mathbf{Z}\mathbf{B}\left(\mathbf{I} - \frac{\mathbf{r}\mathbf{r}^T}{|\mathbf{r}|^2}\right). \tag{12}$$

We observe from (10) that the columns of $\mathbf{M}$ span the tangent space. Let $\mathbf{W}$ denote any $n_s \times n_r$ matrix with $span(\mathbf{W}) = span(\mathbf{M}) = span(\mathbf{T}^{CE})$. Then there exists

a non-singular $n_r \times n_r$ matrix $\mathbf{D}$ such that $\mathbf{T}^{CE} = \mathbf{WD}$. From (5) we obtain

$$\mathbf{B}^T d\mathbf{z}^{CE} = d\mathbf{r} = \mathbf{B}^T \mathbf{T}^{CE} d\mathbf{r} = \mathbf{B}^T \mathbf{W} \mathbf{D} d\mathbf{r}, \quad (13)$$

and hence

$$\mathbf{B}^T \mathbf{T}^{CE} = \mathbf{I}, \quad (14)$$

$$\mathbf{D} = (\mathbf{B}^T \mathbf{W})^{-1}, \quad (15)$$

and finally

$$\mathbf{T}^{CE} = \mathbf{W}(\mathbf{B}^T \mathbf{W})^{-1}. \quad (16)$$

In practice $\mathbf{W}$ is best taken as an orthonormal basis for $span(\mathbf{T}^{CE})$, obtained from the SVD or QR decomposition of $\mathbf{M}$.

It is interesting to observe that $\mathbf{T}^{CE}$ is solely determined by $\mathbf{z}^{CE}$ and $\mathbf{B}$, and does not otherwise depend on any thermodynamic information (such as p, T or $\tilde{\mathbf{g}}$).

B. The ICE Manifold Tangent Vectors

Also important in combining ISAT with ICE-PIC is the matrix of ICE manifold tangent vectors $\mathbf{T}^{ICE}$ defined such that

$$d\mathbf{z}^{ICE} = \mathbf{T}^{ICE} d\mathbf{r}. \quad (17)$$

We are considering now the relevant case of constant pressure and enthalpy, so that (6) and (17) are at fixed p and h. (This implies a re-definition of $\mathbf{T}^{CE}$.)

From (4), considering infinitesimal changes $d\mathbf{r}^g$ and $d\tau$, we have correspondingly

$$d\mathbf{z}^{CE} = \mathbf{T}^{CE} d\mathbf{r}^g, \quad (18)$$

and

$$d\mathbf{z}^{ICE} = \mathbf{A}(\mathbf{z}^g, \tau)\mathbf{T}^{CE}(\mathbf{r}^g) d\mathbf{r}^g + \mathbf{S}(\mathbf{z}^{ICE}) d\tau. \quad (19)$$

We consider the case in which r_k^g is zero on the boundary facet for some value of k. Since we require $\mathbf{r}^g + d\mathbf{r}^g$ to be on the boundary, it follows that dr_k^g is zero. This consideration and (19) show that the tangent space of the ICE manifold is spanned by $\mathbf{S}(\mathbf{z}^{ICE})$ and the $n_r - 1$ vectors obtained from $\mathbf{AT}^{CE}$, with the k-th column omitted. Then, by the same argument that leads to (16), we have

$$\mathbf{T}^{ICE} = \hat{\mathbf{W}}(\mathbf{B}^T \hat{\mathbf{W}})^{-1}, \quad (20)$$

where $\hat{\mathbf{W}}$ is an $n_s \times n_r$ matrix (obtained from $\mathbf{S}$ and $\mathbf{AT}^{CE}$) which spans the ICE manifold tangent space.

IV. Test case: premixed methane combustion

The test case considered is a partially-stirred reactor (PaSR) involving premixed combustion of a methane/air mixture. The PaSR was used previously to investigate ISAT performance [8], [9], [12]. A description of the PaSR is given in [8], [9] and briefly repeated here.

At time t, the PaSR consists of a specified even number N of particles. With Δt being the specified time step, at the discrete times $k\Delta t$ (k integer) events occur corresponding to outflow, inflow, and pairing. Between these discrete times, the composition of particles evolves by a mixing fraction step (with τ_{mix} being the mixing time scale) and a reaction fraction step. With τ_{res} being the specified residence time, outflow and inflow consist of selecting $\frac{1}{2}N\Delta t/\tau_{res}$ pairs at random and replacing their compositions according to inflow compositions, which are drawn from a specified distribution. With τ_{pair} being the specified pairing time scale, $\frac{1}{2}N\Delta t/\tau_{pair}$ pairs of particles (other than the inflow particles) are randomly selected for pairing.

In this study, the GRI-Mech 1.2 mechanism involving 31 species is used to describe the methane combustion. The species involved are

$$\{H_2, H, O_2, OH, H_2O, CH_3, CH_4, CO, CO_2, \quad (21)$$
$$CH_2O, C_2H_4, O, HO_2, H_2O_2, C, CH, CH_2, CH_2(S),$$
$$HCO, CH_2OH, CH_3O, CH_3OH, C_2H, C_2H_2, C_2H_3,$$
$$C_2H_5, C_2H_6, HCCO, CH_2CO, HCCOH, N_2\}$$

The pressure is atmospheric throughout. The specified time scales are $\tau_{res} = 10ms$, $\tau_{mix} = 1ms$, $\tau_{pair} = 1ms$, and the time step is constant with $\Delta t = 0.1ms$. There are two inflowing streams: one premixed stream of air and methane at 600 K and a pilot stream consisting of the adiabatic equilibrium products of a stoichiometric fuel/air mixture at 2375 K (corresponding to an unburnt gas temperature of 600 K). The mass flow rates of the two streams are in the ratio 0.95:0.05. Initially (t = 0), all particle compositions are set to be the pilot-stream composition. The number of particles in the reactor, N, is 100. All the calculations performed result in about 1×10^6 queries.

In the following, we present the results obtained with dimension reduction (DR) methods – both RCCE and ICE-PIC and compare them with the full chemistry (FC) results involving all the species without dimension reduction. Specifically, we present preliminary results on dimension reduction error incurred by RCCE and ICE-PIC, as well as the ISAT statistics indicating the efficiency gains achieved by ISAT.

A. Tabulation error

In the combined DR/ISAT approach, to study the dimension reduction error, the tabulation error incurred by ISAT has to be minimized. We define the tabulation error, ϵ_{tab}, in ISAT in a property, ϕ, at a specified ISAT error tolerance, ϵ_{tol}, for the full chemistry (FC) case to be

$$\epsilon_{tab}(\epsilon_{tol}) = \frac{||\phi_{FC}(\epsilon_{tol}) - \phi_{FC}(\epsilon_{tol}^r)||_2}{max\{|\phi_{FC}(\epsilon_{tol}^r)|\}}, \quad (22)$$

where ϵ_{tol}^r is a small reference error tolerance, which is taken to be $\epsilon_{tol}^r = 10^{-6}$. (Notice that $\epsilon_{tol}^r = 10^{-6}$ is sufficiently small and its corresponding prediction $\phi_{FC}(\epsilon_{tol}^r)$ is regarded to be accurate.) The denominator is the maximum value of the property ϕ with full chemistry over all time.

In this study, the tabulation error incurred by ISAT is calculated by tracking all the particles for all time. Figure1 shows the maximum tabulation error over all the concerned properties (the concentration of all the chemical species in Eq. 21, density, enthalpy and temperature) vs. the ISAT error tolerance (ϵ_{tol}). As can be seen, the tabulation error reaches a very low value of around 0.1%

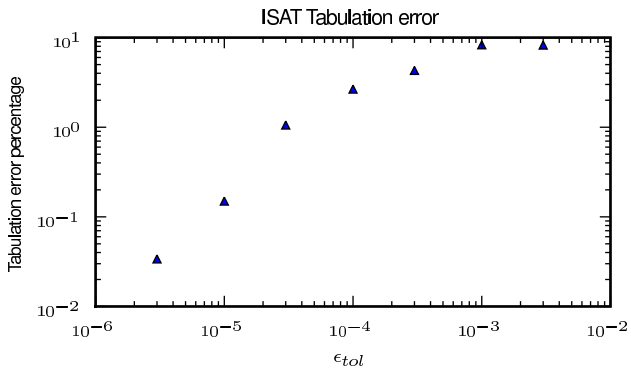

Fig. 1. Plot of the maximum tabulation error in ISAT vs. the specified ISAT error tolerance.

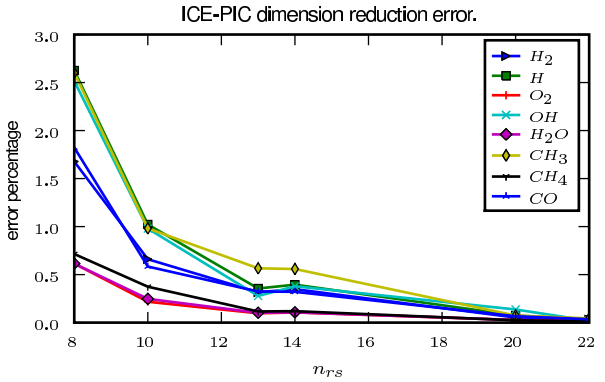

Fig. 3. Plot of the ICE_PIC dimension reduction error in the concentration of the represented species vs. the number of represented species for the methane premixed combustion.

at $\epsilon_{tol} = 10^{-5}$. Hence, it is sufficient to use $\epsilon_{tol} = 10^{-5}$ for studying the dimension reduction errors.

B. Dimension reduction error

We define error, ϵ_{DR}, in a property, ϕ, due to dimension reduction as

$$\epsilon_{DR} = \frac{||\phi_{DR} - \phi_{FC}||_2}{max\{|\phi_{FC}|\}}, \tag{23}$$

where ϕ_{DR} and ϕ_{FC} are the predictions from the reduced description and the full description, respectively (with the ISAT error tolerance $\epsilon_{tol} = 10^{-5}$). The dimension reduction error is calculated by tracking and comparing all the particles for all time.

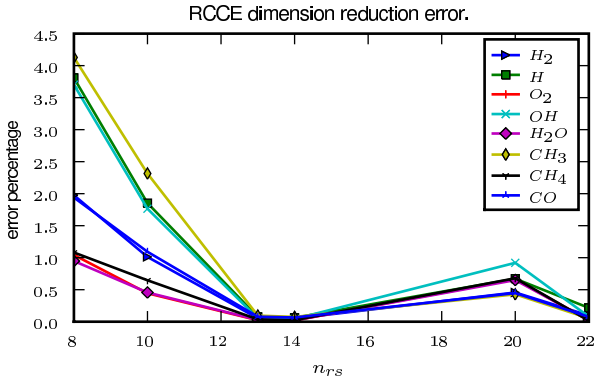

Fig. 2. Plot of the RCCE dimension reduction error in the concentration of the represented species vs. the number of represented species for the methane premixed combustion.

Figures 2 and 3 show the dimension reduction error percentages in the represented species concentrations using the RCCE and ICE-PIC methods respectively. For each reduced description with n_{rs}, the set of first n_{rs} number of species in Eq. 21 are used as the represented species. The errors are computed for the represented species used at the lowest dimension n_{rs} = 8, i.e the first 8 species in Eq. 21 (which are also present in all the higher dimensions). It should be noted that the current approach of choosing the first n_{rs} species as the represented species is not the optimal, and is used only for the convenience of explaining the procedure of dimension reduction error calculation. In future work of ICE-PIC, the best possible set of represented species which give the minimum error would be chosen for a given dimension. As a comparison, Fig.4 shows the maximum dimension reduction error in the concentration of represented species vs. the dimension n_{rs} (number of represented species) for both RCCE and ICE-PIC methods.

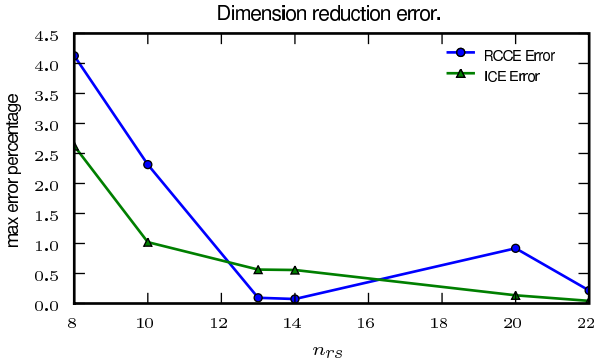

Fig. 4. Plot of the maximum dimension reduction error in the represented species vs. the number of represented species for the methane premixed combustion.

It is readily seen from Figs. 2, 3, 4 that the errors incurred by RCCE and ICE-PIC in the species concentrations are small. For all the cases considered, the maximum dimension reduction error incurred by RCCE and ICE-PIC is about 4% and 2.5%, respectively. Another interesting observation is that as the number of represented species increases, the dimension reduction error incurred by ICE-PIC decreases, but not necessarily so for RCCE. Similar observation can also be made for the errors in the thermodynamic properties such as enthalpy (h) and temperature as shown in Fig.5.

C. ISAT Statistics

In this section we discuss preliminary results for ISAT performance with dimension reduction and compare them

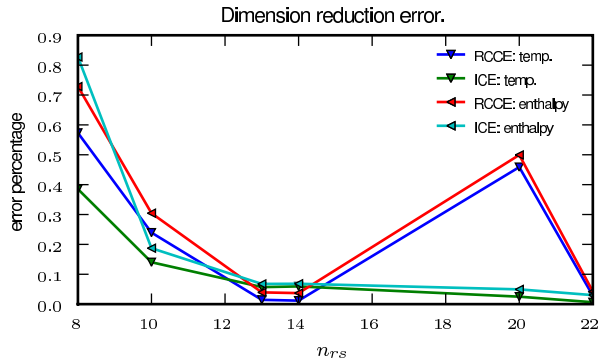

Fig. 5. Plot of the dimension reduction errors in the thermodynamic properties for the methane premixed combustion.

with the full chemistry (no dimension reduction) case. All the calculations (with the ISAT error tolerance $\epsilon_{tol} = 10^{-5}$) result in 1020600 queries to ISAT.

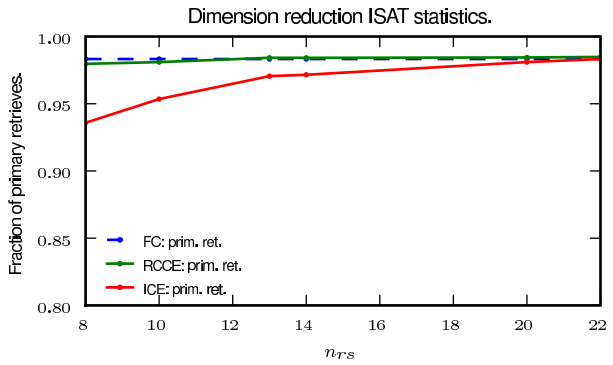

Fig. 6. Plot of fraction of primary retrieves vs. the number of represented species for the methane premixed combustion.

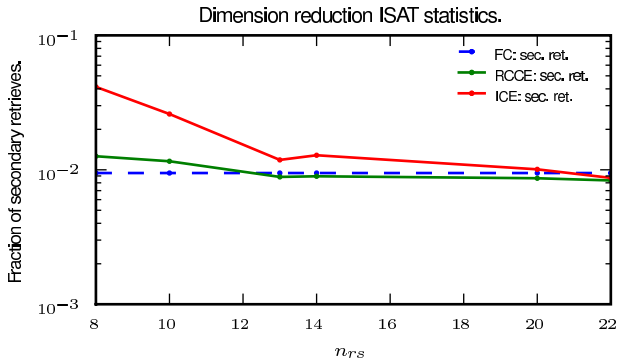

Fig. 7. Plot of fraction of secondary retrieves vs. the number of represented species for the methane premixed combustion.

Figures 6 and 7 show the fraction of queries which resulted in primary and secondary retrieves respectively. And Figs.9, 8 show the fraction of queries that resulted in "adds" and "grows" respectively. It is readily seen that the reduced description by RCCE has comparable

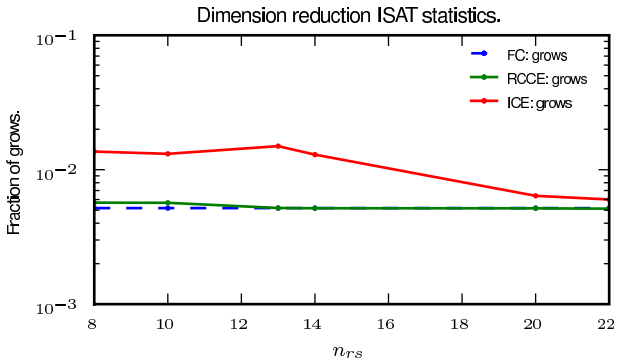

Fig. 8. Plot of fraction of grows vs. the number of represented species for the methane premixed combustion.

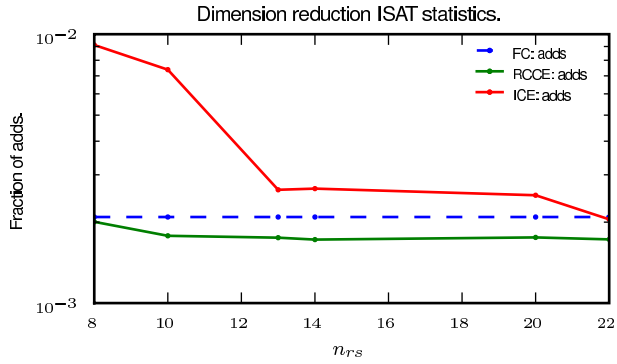

Fig. 9. Plot of fraction of adds vs. the number of represented species for the methane premixed combustion.

ISAT performance as the full description, and most of the queries are successfully resolved by computationally cheap retrieve operations. In contrast, the current implementation of ICE-PIC results in a significant number of computationally expensive grow and add events, particularly with a small number of represented species. The reasons are still under investigation. Future work includes the development of an ICE-PIC implementation with improved ISAT performance.

V. Conclusions

The combination of ICE-PIC and ISAT offers accurate dimension reduction and efficient tabulation. Advances have been made both in the theory (e.g., in the accurate and efficient evaluation of the tangent vectors) and in the computational implementation.

The study shows that the dimension reduction errors in species concentration and thermodynamic properties incurred by ICE-PIC are well controlled and decrease as the number of represented species increases. In the PaSR test case of premixed methane combustion involving 31 species, with 8 represented species, the maximum dimension reduction error incurred by ICE-PIC is only about 2.5%.

Preliminary results for ISAT performance with and without dimension reduction are studied. These show

that the reduced description by RCCE has comparable ISAT performance as the full description, and most of the queries are successfully resolved by computationally cheap retrieve operations. In contrast, the current implementation of ICE-PIC results in a significant number of computationally expensive "grow" and "add" events, particularly with a small number of represented species. The development of an ICE-PIC implementation with improved ISAT performance is in progress.

In future work, a more robust and efficient implementation of ICE-PIC/ISAT will be developed as well as a methodology to choose the optimal represented species, and the application of this combined method in practical combustion calculations is expected.

ACKNOWLEDGMENT

This work is supported by Department of Energy under Grant DE-FG02-90ER and the National Science Foundation under Grant CBET-0426787.

REFERENCES

[1] C.K. Law, Proc. Combust. Inst. 31 (2007) 1-29.
[2] T. Lu, C.K. Law, Proc. Combust. Inst. 30 (2005) 1333-1341.
[3] P. Pepiot, H. Pitsch, Combust. Flame 154 (2008) 61-81.
[4] T. Nagy, T. Turányi, Combust. Flame 156 (2009) 417-428.
[5] Z. Ren, S.B. Pope, A. Vladimirsky, J.M. Guckenheimer, J. Chem. Phys. 124 (2006) 114111.
[6] Z. Ren, S.B. Pope, A. Vladimirsky, J.M. Guckenheimer, Proc. Combust. Inst. 31 (2007) 473-481.
[7] Z. Ren, S.B. Pope, J. Phys. Chem. A 111(34) (2007) 8464-8474.
[8] S.B. Pope, Combust. Theory Modelling 1 (1997) 41-63.
[9] L. Lu, S.B. Pope, J. Comput. Phys. 228 (2009) 361-386.
[10] J.C. Keck, D. Gillespie, Combust. Flame 17 (1971) 237-241.
[11] J.C. Keck, Prog. Energy Combust. Sci. 16 (1990) 125-154.
[12] Q. Tang, S.B. Pope, Proc. Combust. Inst. 29 (2002) 1411-1417.
[13] S.B. Pope, U. Maas, "Simplifying chemical kinetics: trajectory-generated low-dimensional manifolds", Cornell Report FDA 93-11, 1993.
[14] Z. Ren, S.B. Pope, Proc. Combust. Inst. 30 (2005) 1293-1300.
[15] M. Caracotsios, W.E. Stewart, Comput. Chem. Eng. 9(4) (1985) 359-365.
[16] S.B. Pope, Combust. Flame 139 (2004) 222-226.